ORIGINAL ARTICLE

S. Ito
P. C. Ivancic
A. M. Pearson
Y. Tominaga
S. E. Gimenez
W. Rubin
Manohar M. Panjabi

Cervical intervertebral disc injury during simulated frontal impact

S. Ito · P. C. Ivancic · A. M. Pearson
Y. Tominaga · S. E. Gimenez
W. Rubin · M. M. Panjabi (✉)
Biomechanics Research Laboratory,
Department of Orthopedics and
Rehabilitation, Yale University School
of Medicine, 333 Cedar St.,
P.O. Box 208071, New Haven,
Connecticut 06520-8071, USA
E-mail: manohar.panjabi@yale.edu
Tel.: +1-203-7852812
Fax: +1-203-7857069

Abstract Cervical disc injury due to frontal impact has been observed in both clinical and biomechanical investigations; however, there is a lack of data that elucidate the mechanisms of disc injury during these collisions. The goals of the current study were to determine the peak dynamic disc annular tissue strain and disc shear strain during simulated frontal impact of the whole human cervical spine model with muscle force replication at 4 g, 6 g, 8 g and 10 g horizontal accelerations of the T1 vertebra. These data were compared with those obtained during physiological loading, and with previously reported rear impact data. Peak disc shear strain and peak annular tissue strain during frontal impact exceeded ($p < 0.05$) corresponding physiological limits at the C2–C3 intervertebral level, beginning at 4 g and 6 g, respectively. These subsequently spread throughout the entire cervical spine at 10 g, with the exception of C4–C5. The C5–C6 intervertebral level was at high risk for injury during both frontal and rear impacts, while during frontal impact, in addition to C5–C6, subfailure injuries were likely at superior intervertebral levels, including C2–C3. The disc injuries occurred at lower impact accelerations during rear impact as compared with frontal impact. The subfailure injuries of the cervical intervertebral disc that occur during frontal impact may lead to the chronic symptoms reported by patients, such as head and neck pain.

Keywords Spine biomechanics · Cervical disc · Frontal impact · Injury mechanism · Whiplash

Introduction

Soft-tissue injuries have been reported in 23–70% of individuals involved in frontal impacts [1, 28, 34, 35, 54]. Despite this high injury prevalence, the underlying soft-tissue injury mechanisms are not fully understood [55]. The majority of previous frontal impact studies have investigated the response of volunteers [13, 17–20, 27, 36, 40, 57, 59, 60] and cadavers [9, 31, 39, 61] to simulated frontal impacts at accelerations up to 16 g. Among soft-tissue injuries, intervertebral disc injury is often cited as a source of chronic pain [29], via mechanisms of delayed healing or altered loading patterns causing accelerated facet-joint degeneration [8, 25, 37, 56]. Previous autopsy studies have documented disc herniation [28], annulus fiber ruptures [12, 28], and cartilage end-plate separations [56] due to frontal impacts. Frontal impacts may cause subfailure injuries to the soft tissues of the cervical spine, leading to clinical instability and chronic pain [22].

In addition to clinical investigations, biomechanical studies have demonstrated injuries to the disc due to simulated frontal impact. Using a human cervicothoracic model at accelerations up to 15.6 g, Clemens et al. [9] observed fissures and avulsions of the intervertebral disc in 80% of the trials, most commonly at C5–C6. Crowell et al. [11] applied flexion-compression loading to three-vertebra human cervical spine segments and

reported macroscopic annular tears and disc herniations; the disc was the most commonly injured soft-tissue component. Nonetheless, the disc strains were not calculated in either of the previous studies.

Despite previous evidence that has demonstrated disc injury due to actual and simulated frontal impacts, and various studies investigating injury mechanisms due to rear impact [46–48], the injury mechanisms of frontal impact remain poorly understood [55]. Continued biomechanical research may aid in the development of methods to detect, treat and prevent intervertebral disc injuries. Therefore, the goals of this study were to use the whole human cervical spine model with muscle force replication to: (1) determine the dynamic disc annular tissue strain and disc shear strain during simulated frontal impacts, (2) compare these values with limits measured during physiological loading, and (3) compare the present frontal impact data with disc strain data from a previously reported rear impact study.

## Materials and methods

Specimen preparation

Six fresh-frozen human osteoligamentous whole cervical spine specimens were mounted in resin (Fibre Glass-Evercoat, Cincinnati, OH) at the occiput and T1, according to a predefined neutral posture, such that a line from the top of the dens to the lowest point on the posterior occiput was parallel to the occipital mount, while the T1 vertebra was tilted anteriorly by 24° [6]. The average specimen age was 71.3 years (range: 54–87 years), and there were three male and three female donors. The donors did not suffer from any disease that could have affected the osteoligamentous structures. To attach lightweight motion-tracking flags, a headless wood screw was drilled into the anterior aspects of C1 and C2 and into the lamina of C3 through C7. The flags consisted of 3 mm-diameter, hollow brass tubes, with two white, spherical, radio-opaque markers. A flag was fitted rigidly onto each wood screw, and additional flags were attached to the occipital and T1 mounts. This constituted the whole cervical spine (WCS) model prepared for intact flexibility testing.

To prepare a specimen for frontal impact simulation, a surrogate head (mass 3.3 kg and sagittal plane moment of inertia 0.016 kg m^2) was attached to the occipital mount. The head and spine were stabilized using the compressive muscle force replication (MFR) system (Fig. 1). The MFR system was symmetric about the mid-sagittal plane and consisted of anterior, posterior and lateral cables attached to preloaded springs anchored to the base. The stiffness coefficients of the anterior, lateral and posterior tension springs were 4.0 N/mm, 4.0 N/mm and 8.0 N/mm, respectively. Two anterior cables, each consisting of two strands, originated at the occipital mount, ran through separate guideposts at C4, through pulleys within the T1 mount and were each connected to a separate spring. The preload in each anterior spring was 15 N. To apply the posterior MFR, small holes were drilled bilaterally into each lamina (C3 through C7) and wire loops were inserted into the spinal canal through the laminae and tightly secured above each vertebral spinous process. The two posterior MFR cables

Fig. 1 The biofidelic whole cervical spine model (occiput–T1 vertebra) with muscle force replication (WCS + MFR). The surrogate head was attached to the occiput. Anterior, posterior and bilateral MFR cables stabilized the head. The extension head stop is not shown. For more details, please see text
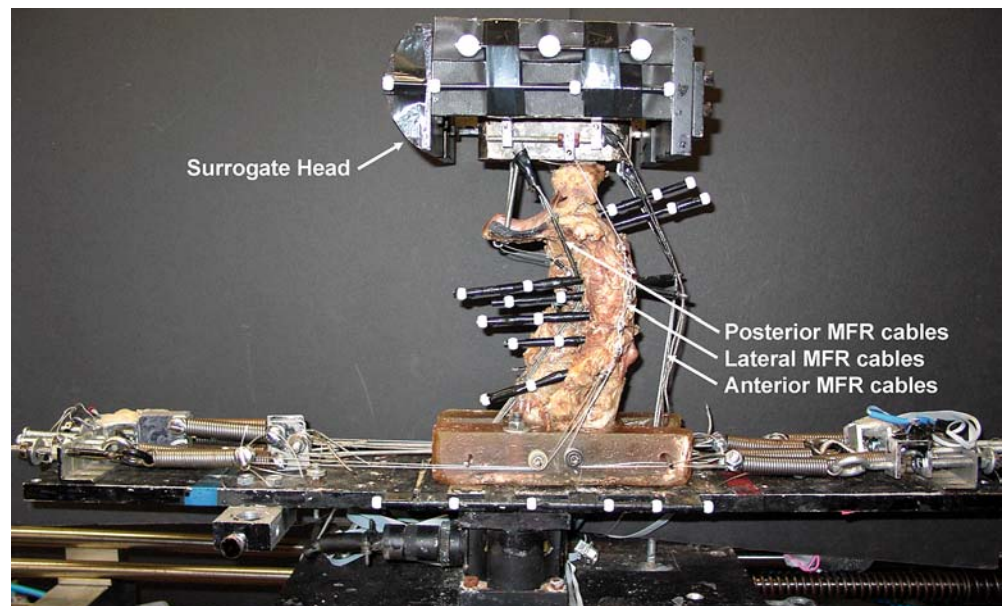
originated from the occipital mount, ran through the wire loops, through a pulley at the T1 mount and each were connected to a spring, preloaded to 15 N. The lateral cables originated from C0, C2, C4, and C6, passed alternately along lateral guide rods, and were each connected to a preloaded 30 N spring. The lateral guide rods were inserted in the frontal plane into the vertebral bodies of C2 through C7, such that the guide rods at C3 through C7 were positioned at the approximate centers of rotation of C2–C3 through C6–C7, respectively. With this MFR arrangement the compressive preloads at each intervertebral level were: 120 N (C0–C1, C1–C2); 180 N (C2–C3, C3–C4); 240 N (C4–C5, C5–C6) and 300 N (C6–C7, C7–T1). A C0–C2 flexion limiter was secured to the occipital mount and to the C2 spinous process that allowed approximately 30° of sagittal rotation, consistent with the in vivo rotation of the normal cervical spine [16, 41]. This constituted the WCS + MFR model, ready for simulated frontal impact (Fig. 1). A lateral X-ray of the WCS + MFR model in the neutral posture, together with radio-opaque calibration markers positioned in the midsagittal plane, was taken and digitally scanned (Adobe Photoshop version 6.01, San Jose, CA).

Intact flexibility testing

The intact WCS model underwent standard flexibility testing to determine the static physiological disc deformations [44]. Pure non-constraining flexion and extension moments up to a maximum of 1.5 Nm were

applied to the occipital mount in four equal steps. Kinematic data were recorded on the third loading cycle, following two preconditioning cycles using a high-speed digital camera (MotionPro, Redlake, MASD, San Diego, CA).

Frontal impact simulation and monitoring

Frontal impact simulation was performed using a previously developed bench-top sled apparatus [45]. The incremental trauma protocol was used to apply frontal impact loading to the WCS + MFR model at nominal T1 maximum horizontal accelerations of 4 g, 6 g, 8 g and 10 g (1 g = 9.81 m/s^2). A head stop was used to restrict head extension during the rebound phase to within physiologic limits and to prevent extension injuries. The high-speed digital camera recorded the spinal motions at 500 frames/s.

Intervertebral disc geometry and deformation

Endplate coordinate system The anterosuperior (point 1) and posterosuperior (point 4) corners of the lower vertebral body of each functional spinal unit from C2–C3 to C6–C7 were selected on the lateral X-ray (Fig. 2). Two additional points (points 2 and 3) were selected, such that the point 2 was midway between points 1 and 4, and point 3 was midway between points 2 and 4. The endplate coordinate system *y-z* had its origin at point 4,

Fig. 2 Functional spinal unit with motion tracking flags and the points on the endplates used to calculate intervertebral disc deformation. Two coordinate systems are also shown. The endplate coordinate system *y-z* was fixed to the lower vertebral body. The anterior (2–A) and middle (3–B) annular tissues are shown by *dashed lines*, while the posterior annular tissue (4–C) is shown by a *solid line*. The points (1′, 2′ and 4′) were selected on the inferior surface of the upper vertebral body that were directly above points 1, 2 and 4, respectively, and were used to calculate the disc shear strain at the anterior, middle and posterior disc regions. The ground coordinate system *h-v* defined flexion as positive rotation
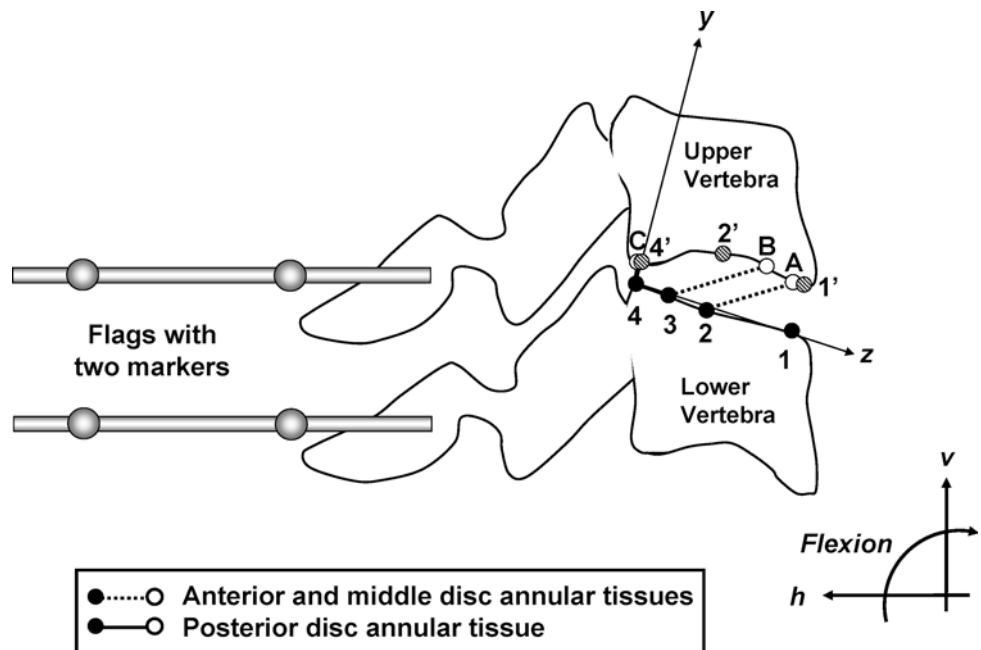
its positive z-axis was oriented anteriorly through point 1, and its positive y-axis was orthogonal to the z-axis and oriented superiorly.

Disc annular tissue strain The superficial anterior annular tissue of the cervical disc and the deepest alar tissues of the anterior longitudinal ligament have been described in three dimensions as running posteroinferiorly and laterally from the upper to the lower vertebral body [38], at approximately 30° to the z-axis. The thin, superficial posterior annular tissue has been described as having a longitudinal orientation [38]. These tissues were most likely to be loaded due to flexion during frontal impact simulations, and thus were mathematically constructed to develop a sagittal plane disc model based on the lateral X-ray. The anterior and middle annular tissues had origins at points 2 and 3, respectively, and insertions at the inferior surface of the upper vertebral body (points A and B, respectively), and were oriented at 30° to the z-axis (Fig. 2). The posterior annular tissue was oriented vertically and had its origin at point 4 and insertion at the posteroinferior corner of the upper vertebral body (point C).

Geometrical rigid body relationships between the flag markers and the annular tissue origins and insertions were digitized for each specimen from the scanned X-rays and were superimposed onto the first frame of the high-speed movie. Custom Matlab motion-tracking software, written with sub-pixel accuracy, computed the vertebral body rotations and flag marker translations at each subsequent frame in the ground coordinate system *h-v* (Fig. 2). These data, together with the geometrical rigid body relationships, were used to track the selected points and to calculate the translation of the annular tissue origins and insertions in the ground coordinate system *h-v* throughout frontal impact simulation. To compute the dynamic annular tissue strains, the change in tissue length was expressed as a percentage of the original tissue length in neutral posture. The physiological tissue strain was defined as the peak value obtained during the flexibility testing. The average error in the system used to calculate disc deformations was 0.3 mm (SD 0.2 mm), and, consequently, the average strain error was approximately 3.0% (SD 2.0%) [51].

Disc shear strain Three additional points (1′, 2′ and 4′) were selected on the inferior surface of the upper vertebral body such that 1′, 2′ and 4′ were directly superior (positive y-coordinate) to points 1, 2 and 4, respectively (Fig. 2). These points, representative of the anterior, middle and posterior disc regions, were tracked throughout simulated frontal impact using the custom motion-tracking software and the rigid body relationships between the flag markers and the points. The points were used to calculate the disc shear strain (γ) at each of the three locations:

$$\gamma = \arctan\left(\frac{\Delta z}{y_0}\right) \quad (1)$$

where Δz represented the z-axis translation of 1′, 2′ and 4′ relative to 1, 2 and 4, respectively. The original disc heights (y_0) were obtained as the y-axis differences between 1′, 2′ and 4′ and 1, 2 and 4, on the neutral posture lateral X-ray. Corresponding physiological limits were defined as the maximum values obtained during the flexibility testing.

Data analyses

Disc strain data were low-pass digitally filtered at a 30 Hz cut-off frequency. For each frontal impact simulation, the peak anterior, middle and posterior disc annular tissue strains and disc shear strains were determined for each intervertebral level (C2–C3 to C6–C7) during the total intervertebral flexion time period (i.e., from the T1 horizontal acceleration onset to return to the neutral posture, after maximum intervertebral flexion). Single factor, repeated measures analysis of variance (ANOVA) ($p < 0.05$) and Bonferroni post hoc tests (Minitab Release 13, State College, PA, USA) were used to compare peak annular tissue strain and disc shear strain during simulated frontal impact, with the corresponding physiological limits determined from the flexibility testing.

Results

The average measured peak T1 horizontal accelerations during the frontal impact simulations were 3.9 g, 5.7 g, 8.5 g, and 10.0 g (ΔV: 8.4 kph, 11.4 kph, 13.4 kph, and 13.8 kph), corresponding to the nominal maximum accelerations of 4 g, 6 g, 8 g, and 10 g, respectively. The average T1 horizontal acceleration pulse duration was 107.3 ms, and this compared favorably with values measured during real-life collisions, ranging between approximately 70 ms and 100 ms [5].

An example of disc strains during frontal impact

The disc kinematics varied among intervertebral levels and specimens. An example of disc strains as functions of time is provided by the C2–C3 disc of specimen No. 1 during the 6 g frontal impact (Fig. 3). Two phases, based on intervertebral rotation, were defined. Phase I began with the onset of T1 horizontal acceleration (time 0 ms) and concluded with peak intervertebral flexion, while phase II spanned from peak intervertebral flexion to the return of neutral posture. The anterior annular

Fig. 3 An example of disc strains during frontal impact showing anterior and posterior disc annular tissue strain (*2–A* and *4–C*, Fig. 2), posterior region disc shear strain, and intervertebral flexion. The results are of specimen No. 1 at level C2–C3 during the 6 g frontal impact
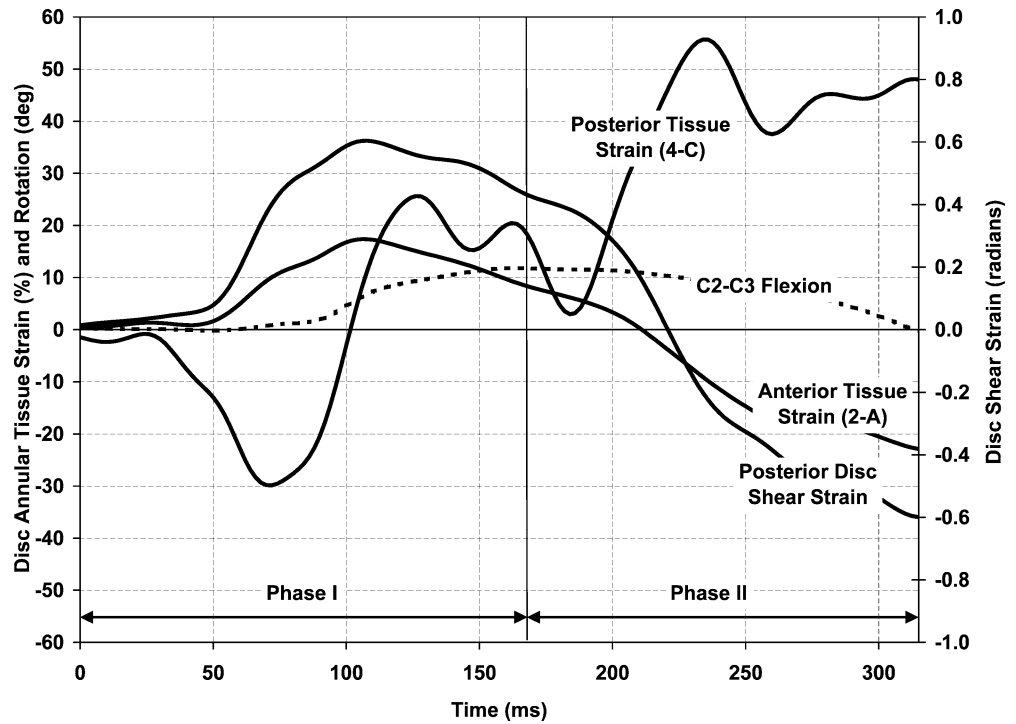
tissue strain and posterior disc shear strain increased and peaked in phase I, and returned towards zero in phase II. The posterior annular tissue strain peaked in phase II, following maximum intervertebral flexion.

Average behavior of six specimens

The dynamic disc annular tissue strains and disc shear strains are presented in Tables 1 and 2, where exact means of neutral tissue length, neutral disc height, and

strain values with corresponding standard deviations are provided. The data are also presented as three-dimensional graphs together with the corresponding physiological limits. These provide an overview of their variance by anatomical location, intervertebral level and impact acceleration (Figs. 4 and 5).

The C2–C3 middle disc annular tissue strain first exceeded physiological limits at 6 g and subsequently spread to all intervertebral levels at 10 g, excluding C4–C5 (Table 1, Fig. 4). At 10 g, anterior annular tissue strain exceeded the physiological limits throughout the

Table 1 Peak disc annular tissue strains. Average (SD) neutral tissue lengths (mm) and peak annular tissue strains (%) during physiological flexion limits and simulated frontal impact at anterior (*Ant*), middle (*Mid*) and posterior (*Post*) regions of the disc, at

intervertebral levels C2–C3 through C6–C7 (see Fig. 2). Significant increases ($p < 0.05$) in the frontal impact strains over the corresponding physiological limits are indicated by *

Level	C2–C3			C3–C4			C4–C5			C5–C6			C6–C7		
Region	Ant	Mid	Post	Ant	Mid	Post	Ant	Mid	Post	Ant	Mid	Post	Ant	Mid	Post
Neutral length	8.4	7.1	3.2	8.4	7.1	2.9	8.4	7.3	3.1	6.9	6.0	3.0	7.4	6.3	3.0
	(0.9)	(3.2)	(0.5)	(1.3)	(3.0)	(1.0)	(1.0)	(3.2)	(0.7)	(1.7)	(2.7)	(0.8)	(0.8)	(2.8)	(0.4)
Physiological limits	13.1	9.9	52.3	13.4	12.2	81.7	14.1	10.1	39.2	9.9	7.9	48.8	10.5	6.7	28.4
	(8.4)	(5.3)	(30.8)	(7.3)	(6.8)	(20.4)	(13.0)	(8.7)	(32.3)	(6.4)	(5.6)	(24.9)	(12.8)	(8.0)	(24.8)
4 g impact	24.7	24.2	37.4	7.8	7.8	50.7	8.2	8.1	29.1	5.9	6.7	38.4	8.3	8.7	62.9
	(18.1)	(15.7)	(20.7)	(5.3)	(5.4)	(35.0)	(5.4)	(4.6)	(15.4)	(6.5)	(7.1)	(18.1)	(9.0)	(9.3)	(21.4)
6 g impact	34.1	32.8*	50.5	6.7	7.0	46.1	9.3	9.6	61.3	5.7	7.0	48.6	5.7	6.8	31.9
	(23.6)	(20.7)	(22.7)	(8.4)	(7.8)	(33.9)	(8.2)	(7.9)	(27.7)	(3.6)	(4.3)	(28.1)	(8.7)	(10.0)	(9.6)
8 g impact	39.7	38.4*	33.0	7.3	7.4	62.5	14.6	14.2	42.8	6.7	8.0	75.4	8.4	9.6	48.6
	(30.7)	(28.8)	(18.3)	(7.3)	(7.5)	(50.5)	(16.8)	(14.9)	(14.4)	(2.6)	(3.6)	(61.7)	(12.0)	(12.4)	(10.8)
10 g impact	43.1*	39.9*	44.6	23.7	23.2*	116.5*	24.4	22.8	54.9	29.6*	28.6*	105.6*	19.7*	20.6*	46.0
	(29.4)	(25.6)	(35.8)	(9.8)	(6.6)	(36.1)	(19.8)	(17.6)	(34.9)	(12.8)	(10.4)	(49.5)	(10.0)	(9.2)	(23.3)

Table 2 Peak disc shear strains. Average (SD) neutral disc heights (mm) and peak disc shear strains (radians) during physiological flexion limits and simulated frontal impact at the anterior (*Ant*), middle (*Mid*) and posterior (*Post*) regions of the disc (see Fig. 2), at intervertebral levels C2–C3 through C6–C7. Significant increases ($p < 0.05$) in the frontal impact strains over the corresponding physiological limits are indicated by *

Level	C2–C3			C3–C4			C4–C5			C5–C6			C6–C7		
Region	Ant	Mid	Post	Ant	Mid	Post	Ant	Mid	Post	Ant	Mid	Post	Ant	Mid	Post
Neutral height	4.7	5.5	3.2	4.4	5.6	2.9	4.6	5.5	3.1	3.5	4.6	3.0	3.6	4.6	3.0
	(0.9)	(0.4)	(0.5)	(1.0)	(0.9)	(1.0)	(0.8)	(0.7)	(0.7)	(1.2)	(1.4)	(0.8)	(0.9)	(0.7)	(0.4)
Physiological limits	0.3	0.2	0.4	0.2	0.2	0.3	0.3	0.3	0.4	0.2	0.2	0.2	0.2	0.2	0.3
	(0.1)	(0.1)	(0.1)	(0.1)	(0.1)	(0.2)	(0.2)	(0.2)	(0.3)	(0.2)	(0.1)	(0.2)	(0.3)	(0.3)	(0.3)
4 g impact	0.6*	0.5*	0.7*	0.2	0.2	0.3	0.2	0.2	0.3	0.2	0.2	0.2	0.2	0.2	0.2
	(0.2)	(0.2)	(0.2)	(0.1)	(0.1)	(0.2)	(0.1)	(0.1)	(0.2)	(0.2)	(0.2)	(0.3)	(0.2)	(0.2)	(0.2)
6 g impact	0.7*	0.6*	0.9*	0.2	0.2	0.3	0.3	0.3	0.4	0.2	0.2	0.3	0.3	0.2	0.3
	(0.2)	(0.2)	(0.2)	(0.2)	(0.2)	(0.3)	(0.2)	(0.2)	(0.3)	(0.2)	(0.2)	(0.3)	(0.3)	(0.2)	(0.3)
8 g impact	0.8*	0.7*	1.0*	0.2	0.2	0.3	0.3	0.3	0.4	0.2	0.3	0.4	0.4	0.3	0.4
	(0.2)	(0.2)	(0.2)	(0.2)	(0.2)	(0.3)	(0.2)	(0.2)	(0.3)	(0.1)	(0.1)	(0.2)	(0.2)	(0.2)	(0.3)
10 g impact	0.7*	0.6*	0.8*	0.4*	0.4*	0.5	0.5	0.4	0.6	0.5*	0.5*	0.7*	0.7*	0.6*	0.7*
	(0.3)	(0.3)	(0.3)	(0.2)	(0.2)	(0.3)	(0.3)	(0.2)	(0.3)	(0.2)	(0.2)	(0.2)	(0.2)	(0.2)	(0.2)

Fig. 4 Average peak anterior (*Ant*), middle (*Mid*) and posterior (*Post*) disc annular tissue strains at C2–C3 through C6–C7 during simulated frontal impact (4 to 10 g) and physiological limits. Significant increases ($p < 0.05$) in frontal impact strains over the corresponding physiological limits are indicated by *
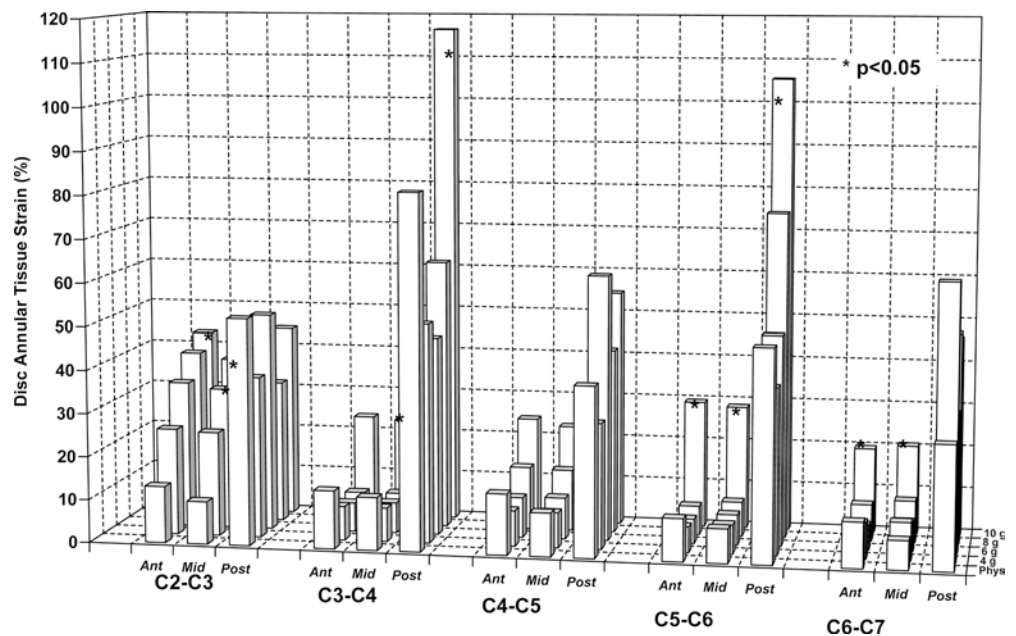
cervical spine, with the exception of C3–C4 and C4–C5. The highest peaks for the anterior and middle annular tissue strains occurred at 10 g. These were 43.1% and 39.9% at C2–C3 and 29.6% and 28.6% at C5–C6, respectively. The posterior annular tissue strains beyond the corresponding physiological limits were observed at C3–C4 (116.5%) and C5–C6 (105.6%), both during the 10 g impact.

Disc shear strain at C2–C3 exceeded physiological limits beginning at 4 g (Table 2 and Fig. 5). At 10 g, increases in disc shear strain were observed at all intervertebral levels, excluding C4–C5. Of these increases, the greatest disc shear strain was most often noted in the posterior disc region, reaching 0.9 radians and 1.0 radians (125% and 150% increases from physiological limits) at C2–C3, during the 6 g and 8 g impacts, respectively.

Discussion

Injuries to the cervical disc sustained during automobile collisions may result in chronic pain [23, 24, 29], yet there are currently no biomechanical studies investigating disc injury mechanisms during simulated frontal impact. The present study determined the dynamic disc

Fig. 5 Average peak disc shear strains at the anterior (*Ant*), middle (*Mid*), and posterior (*Post*) disc regions of C2–C3 through C6–C7 during simulated frontal impact and physiological limits. Significant increases ($p < 0.05$) in frontal impact strains over the corresponding physiological limits are indicated by *
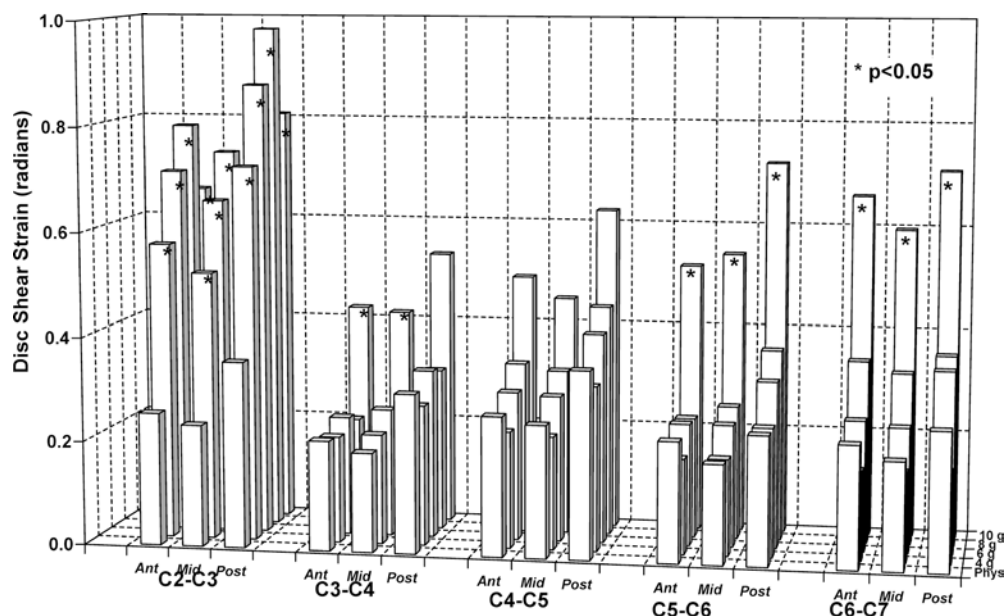
annular tissue strain and disc shear strain during simu-
lated frontal impact, using a biofidelic whole cervical
spine model with muscle force replication. At 4 g and
6 g, significant increases ($p < 0.05$) over physiological
limits were observed in the C2–C3 disc shear strains and
middle disc annular tissue strains, respectively. The
largest disc shear strain was observed in the posterior
disc region, reaching a maximum of 1.0 radian (150%
increase over the physiological limit) at C2–C3 during
the 8 g impact. At 10 g, anterior disc annular tissue
strains exceeded physiological limits at all intervertebral
levels, excluding C3–C4 and C4–C5, while the posterior
annular tissue strains exceeded physiological limits at
C3–C4 and C5–C6. The disc annular tissue strain and
disc shear strain results suggest that during frontal
impact, intervertebral flexion combined with disc
shearing may be the injury mechanism producing
subfailure disc injuries. In support of these findings,
previous clinical hypotheses have suggested that frontal
impact would likely produce horizontal shear between
cervical vertebrae, and result in excessive strain of the
anterior disc annular tissues with compression of
zygapophysial joints [2, 58].

There are several limitations of the present model
that must be considered. Firstly, the T1 vertebra was
fixed to the sled, which may have affected the cervical
spine kinematics, especially at C7–T1. While no data
exist that quantify the in vivo intervertebral rotations
during simulated frontal impact, the peak head-T1
flexion of young volunteers with pre-tensed muscles
ranged between 49.4° and 74.0° during simulated frontal
collisions up to 15.6 g [57]. The average (SD) peak head-
T1 flexion of the present study ranged from 43.1° (5.9°)
to 84.6° (6.0°), during the 4 g and 10 g impacts,

respectively, and exceeded the in vivo corridor, since the
current model simulated the response of an unwarned
subject. Secondly, the incremental trauma approach was
used to determine the relationship between disc strain
and impact acceleration. The many advantages of the
incremental trauma protocol have been well documented
[26, 48]. The incremental and single trauma protocols
have been shown to produce equivalent soft-tissue injury
severity due to frontal impacts of a porcine cervical spine
model [21]. In that study, the incremental trauma group
underwent 2 g, 3.5 g, 5 g, 6.5 g and 8 g impacts, while
the single trauma group underwent only the 8 g impact.
Flexibility testing was performed on each specimen
while intact, and following each impact. There were no
statistically significant differences in the flexibility
parameters between the incremental and single trauma
groups following the 8 g impacts. This well-controlled
experiment validates the use of the incremental trauma
protocol for determining disc strains due to frontal
impact. Lastly, the current model did not simulate an
active neuromuscular response: the MFR system pro-
vided postural stability and passive resistance to inter-
vertebral motion following impact, simulating the
response of an unwarned occupant. While individuals
may be able to anticipate frontal collisions, they may not
be able to generate adequate neck muscle force to
restrict head flexion. The average peak extension mo-
ment of 18.7 Nm at C7–T1 produced by the present
MFR exceeds the peak extension moment developed by
weaker subjects (in vivo female range: 9 to 33 Nm) [49].
In addition to not being able to generate enough force to
resist motion, the muscles may not be able to achieve
peak tension quickly enough to protect the cervical spine
from injury. The peak disc annular tissue strain and disc

shear strain of the current study occurred between 148.5 ms and 151.3 ms, respectively, following impact. A recent study measured the electromyographic activity of the cervical muscles during simulated frontal impacts up to 1.4 g and found that the trapezius muscle was the first to achieve peak activity at 189 ms following impact [36]. Thus, the posterior cervical muscles may neither be able to develop sufficient strength, nor respond quickly enough to restrict head flexion or protect the neck following frontal impact.

Comparison of the current frontal impact disc shear strain data to previously reported rear impact data [50] revealed differing intervertebral levels at risk for injury (Fig. 6). The C2–C3 intervertebral level displayed greater increases during frontal impact, while in rear impact, C5–C6 was at the greatest risk. Although studies have demonstrated injuries to the C2–C3 disc during frontal impacts [9, 28, 56], a larger body of evidence notes that the C5–C6 intervertebral level is most commonly injured in both frontal and rear impact collisions [9, 12, 29, 32, 52, 62]. The injuries at C5–C6 during frontal impact occurred at 10 g, while injuries due to rear impact began at 3.5 g. This observation concurs with epidemiological evidence, which suggests that injuries may occur at lower impact accelerations during rear impact, as compared with frontal impact [34, 53, 55]. The data of the current study suggest that injuries observed at C2–C3 and C5–C6 might be due to the increases in disc annular tissue strain and disc shear strain beyond the physiological limits.

Understanding how subfailure injuries may cause pain is perhaps the most important issue when investigating disc injuries sustained during frontal impact. Apart from neck pain, headache is the most commonly reported symptom following frontal and rear impacts [2, 53]. Occipital or cervicogenic headache is known to result from referred pain via injury to the C2–C3 zygapophysial joint, which is innervated by the third occipital nerve [2, 3, 30]. Injury to the C2–C3 disc, suggested by the present study, may lead to accelerated degenerative changes over time, and abnormal loading of the adjacent zygapophysial joints [8]. Frontal impact patients may be at higher risk for occipital headaches and thus obtain relief from therapeutics targeting the occipital nerve [14, 15]. Other sources of chronic pain from subfailure injuries have been ascribed to mechanisms directly involving the disc, such as the presence of injured nociceptive fibers on the annulus fibrosus [4, 10], and the subsequent production of irritative inflammatory mediators [7, 33]. A final, commonly proposed pain mechanism is the accelerated degeneration of the injured disc, leading to facet degeneration and painful facet inflammation [8, 42, 43].

Conclusions

The present study demonstrated that disc annular tissue strain and disc shear strain exceeded physiological limits during simulated frontal impact. These data suggest that subfailure disc injuries that occur during frontal impact might be caused by combined intervertebral flexion and disc shearing. A comparison to previously reported rear impact data revealed that the C5–C6 intervertebral disc was at the greatest injury risk during rear impact, while during frontal impact, in addition to C5–C6, subfailure injuries are likely at superior intervertebral levels, including C2–C3. The disc injuries occurred at lower

Fig. 6 Comparison of peak disc shear strain during frontal and rear impact [50] at 8 g (C2–C3 through C6–C7)
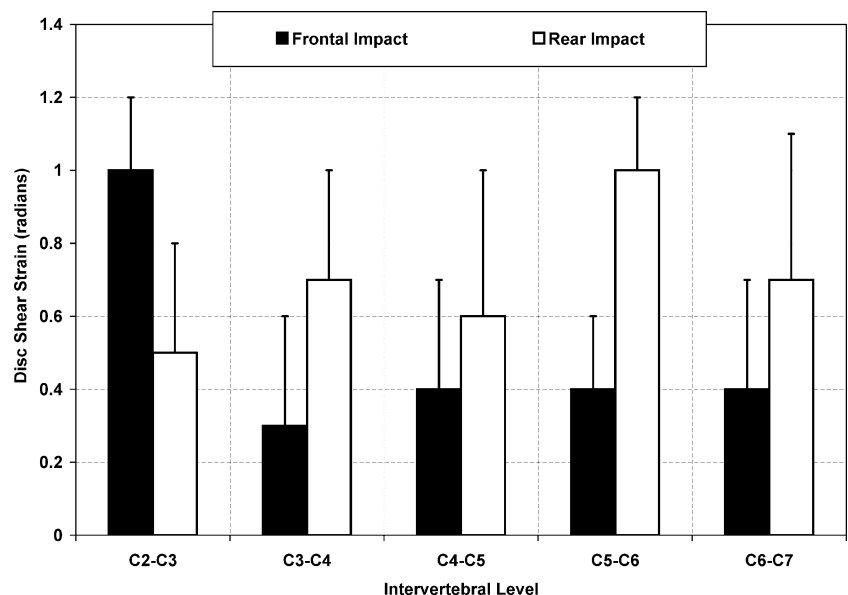
impact accelerations during rear impact, as compared with frontal impact. Disc injuries may be a source of chronic pain following both frontal and rear impacts.

References

1. Allen BL Jr, Ferguson RL, Lehmann TR, O'Brien RP (1982) A mechanistic classification of closed, indirect fractures and dislocations of the lower cervical spine. Spine 7:1–27
2. Barnsley L, Lord S, Bogduk N (1994) Whiplash injury. Pain 58:283–307
3. Bogduk N, Marsland A (1986) On the concept of third occipital headache. J Neurol Neurosurg Psychiatry 49:775–80
4. Bogduk N, Windsor M, Inglis A (1988) The innervation of the cervical intervertebral discs. Spine 13:2–8
5. Bostrom O, Bohman K, Haland Y, Kullgren A (2000) New AIS1 long-term neck injury criteria candidates based on real frontal crash analysis. International Research Council on the Biomechanics of Impact. Montpelier, France, 249–280
6. Braakman R, Penning L (1971) Injuries of the cervical spine. Excelptra Media, Netherlands
7. Burke JG, Watson RW, McCormack D et al (2002) Intervertebral discs which cause low back pain secrete high levels of proinflammatory mediators. J Bone Joint Surg Br 84:196–201
8. Butler D, Trafimow JH, Andersson GB, McNeill TW, Huckman MS (1990) Discs degenerate before facets. Spine 15:111–113
9. Clemens HJ, Burow K (1972) Experimental investigation on injury mechanisms of cervical spine at frontal and rear-front vehicle impacts. Society of Automotive Engineers, paper No. 720960
10. Coppes MH, Marani E, Thomeer RT, Groen GJ (1997) Innervation of "painful" lumbar discs. Spine 22:2342–2349
11. Crowell RR, Shea M, Edwards WT et al (1993) Cervical injuries under flexion and compression loading. J Spinal Disord 6:175–181
12. Davis SJ, Teresi LM, Bradley WG Jr, Ziemba MA, Bloze AE (1991) Cervical spine hyperextension injuries: MR findings. Radiology 180:245–251
13. deJager M, Sauren A, Thunnissen J, Wismans J (1994) A three-dimensional head-neck model: validation for frontal and lateral Impacts. Society of Automotive Engineers, paper No. 942211
14. Drottning M (2003) Cervicogenic headache after whiplash injury. Curr Pain Headache Rep 7:384–386

15. Drottning M, Staff PH, Sjaastad O (2002) Cervicogenic headache (CEH) after whiplash injury. Cephalalgia 22:165–171
16. Dvorak J, Panjabi MM, Novotny JE, Antinnes JA (1991) In vivo flexion/ extension of the normal cervical spine. J Orthop Res 9:828–834
17. Ewing CL, Thomas DJ, Beeler GW, Patrick LM, Gillis DB (1968) Dynamic response of the head and neck of the living human to -Gx impact acceleration. Society of Automotive Engineers, paper No. 680792
18. Ewing CL, Thomas DJ, Patrick LM, Beeler GW, Smith MJ (1969) Living human dynamic response to -Gx impact acceleration: Part II accelerations measured on the head and neck. Society of Automotive Engineers, paper No. 690817
19. Ewing CL, Thomas DJ, Lustick L et al (1975) The effect of the initial position of the head and neck on the dynamic response of the human head and neck to -gx impact acceleration. Society of Automotive Engineers, paper No. 751157
20. Ewing CL, Thomas DJ, Lustick L et al (1976) The effect of duration, rate of onset and peak sled acceleration on the dynamic response of the human head and neck. Society of Automotive Engineers, paper No. 760800
21. Ghole SA, Ivancic PC, Tominaga Y, Gimenez SE, Panjabi MM (2004) Incremental and single trauma produce equivalent subfailure soft tissue injury of the cervical spine. Clin Biomech (Bristol, Avon) 19:784–789
22. Herkowitz HN, Rothman RH (1984) Subacute instability of the cervical spine. Spine 9:348–357
23. Hohl M (1974) Soft-tissue injuries of the neck in automobile accidents. Factors influencing prognosis. J Bone Joint Surg Am 56:1675–1682
24. Hohl M (1975) Soft tissue injuries of the neck. Clin Orthop:42–49
25. Hsieh AH, Lotz JC (2003) Prolonged spinal loading induces matrix metalloproteinase-2 activation in intervertebral discs. Spine 28:1781–1788
26. Ito S, Ivancic PC, Panjabi MM, Cunningham BW (2004) Soft tissue injury threshold during simulated whiplash: a biomechanical investigation. Spine 29:979–987

27. Ivancic PC, Pearson AM, Panjabi MM, Ito S (2004) Injury of the anterior longitudinal ligament during whiplash simulation. Eur Spine J 13:61–68
28. Jonsson H, Bring G, Rauschning W, Sahlstedt B (1991) Hidden cervical spine injuries in traffic accident victims with skull fractures. J Spinal Disord 4:251–263
29. Jonsson H, Cesarini K, Sahlstedt B, Rauschning W (1994) Findings and outcome in whiplash-type neck distortions. Spine 19:2733–2743
30. Jull G, Bogduk N, Marsland A (1988) The accuracy of manual diagnosis for cervical zygapophysial joint pain syndromes. Med J Aust 148:233–236
31. Kallieris D, Mattern R, Miltner E, Schmidt MH, Stein K (1991) Considerations for a neck injury criterion. Society of Automotive Engineers, paper No. 912916
32. Kaneoka K, Ono K, Inami S, Hayashi K (1999) Motion analysis of cervical vertebrae during whiplash loading. Spine 24:763–769
33. Kang JD, Stefanovic-Racic M, McIntyre LA, Georgescu HI, Evans CH (1997) Toward a biochemical understanding of human intervertebral disc degeneration and herniation. Contributions of nitric oxide, interleukins, prostaglandin E2, and matrix metalloproteinases. Spine 22:1065–1073
34. Krafft M, Kullgren A, Lie A, Nygren A, Tingvall C (1997) Soft tissue injury of the cervical spine in rear-end car collisions. J Traff Med 25 Nos. 3–4:89–96
35. Kullgren A, Krafft M, Nygren A, Tingvall C (2000) Neck injuries in frontal impacts: influence of crash pulse characteristics on injury risk. Accid Anal Prev 32:197–205
36. Kumar S, Narayan Y, Amell T (2003) Analysis of low velocity frontal impacts. Clin Biomech (Bristol, Avon) 18:694–703
37. Leonardi M, Simonetti L, Agati R (2002) Neuroradiology of spine degenerative diseases. Best Pract Res Clin Rheumatol 16:59–87
38. Mercer S, Bogduk N (1999) The ligaments and annulus fibrosus of human adult cervical intervertebral discs. Spine 24:619–626

39. Mertz HJ, Patrick LM (1967) Investigation of the kinematics and kinetics of whiplash. Society of Automotive Engineers, paper No. 670918
40. Mertz HJ, Patrick LM (1971) Strength and response of the human neck. Society of Automotive Engineers, paper No. 710855
41. Ordway NR, Seymour RJ, Donelson RG, Hojnowski LS, Edwards WT (1999) Cervical flexion, extension, protrusion, and retraction. A radiographic segmental analysis. Spine 24:240–247
42. Osti OL, Vernon-Roberts B, Fraser RD (1990) 1990 Volvo Award in experimental studies. Anulus tears and intervertebral disc degeneration. An experimental study using an animal model. Spine 15:762–767
43. Osti OL, Vernon-Roberts B, Moore R, Fraser RD (1992) Annular tears and disc degeneration in the lumbar spine. A post-mortem study of 135 discs. J Bone Joint Surg Br 74:678–682
44. Panjabi MM, Oxland TR, Lin RM, McGowen TW (1994) Thoracolumbar burst fracture. A biomechanical investigation of its multidirectional flexibility. Spine 19:578–585
45. Panjabi MM, Cholewicki J, Nibu K, Babat LB, Dvorak J (1998) Simulation of whiplash trauma using whole cervical spine specimens. Spine 23:17–24
46. Panjabi MM, Cholewicki J, Nibu K, Grauer J, Vahldiek M (1998) Capsular ligament stretches during in vitro whiplash simulations. J Spinal Disord 11:227–232
47. Panjabi MM, Cholewicki J, Nibu K et al (1998) Mechanism of whiplash injury. Clin Biomech (Bristol, Avon) 13:239–249
48. Panjabi MM, Nibu K, Cholewicki J (1998) Whiplash injuries and the potential for mechanical instability. Eur Spine J 7:484–492
49. Panjabi MM, Crisco JJ, Vasavada A et al (2001) Mechanical properties of the human cervical spine as shown by three-dimensional load-displacement curves. Spine 26:2692–2700
50. Panjabi MM, Ito S, Pearson AM, Ivancic PC (2004) Injury mechanisms of the cervical intervertebral disc during simulated whiplash. Spine 29:1217–1225
51. Pearson AM, Ivancic PC, Ito S, Panjabi MM (2004) Facet joint kinematics and injury mechanisms during simulated whiplash. Spine 29:390–397
52. Pettersson K, Hildingsson C, Toolanen G, Fagerlund M, Bjornebrink J (1997) Disc pathology after whiplash injury. A prospective magnetic resonance imaging and clinical investigation. Spine 22:283–287
53. Radanov BP, Sturzenegger M, Di Stefano G (1995) Long-term outcome after whiplash injury. A 2-year follow-up considering features of injury mechanism and somatic, radiologic, and psychosocial findings. Medicine 74:281–297
54. Richter M, Otte D, Pohlemann T, Krettek C, Blauth M (2000) Whiplash-type neck distortion in restrained car drivers: frequency, causes and long-term results. Eur Spine J 9:109–117
55. Spitzer WO, Skovron ML, Salmi LR et al (1995) Scientific monograph of the Quebec Task Force on Whiplash-Associated Disorders: redefining "whiplash" and its management. Spine 20:1S-73S
56. Taylor JR, Twomey LT (1993) Acute injuries to cervical joints. An autopsy study of neck sprain. Spine 18:1115–1122
57. Thunnissen J, Wismans J, Ewing CL, Thomas DJ (1995) Human volunteer head-neck response in frontal flexion: a new analysis. Society of Automotive Engineers, paper No. 952721
58. Walz FH, Muser MH (1995) Biomechanical aspects of cervical spine injuries. Society of Automotive Engineers, paper No. 950658
59. Wismans J, Spenny CH (1984) Head-neck response in frontal flexion. Society of Automotive Engineers, paper No. 841666
60. Wismans J, van Oorschot H, Woltring HJ (1986) Omni-directional human head-neck response. Society of Automotive Engineers, paper No 861893
61. Wismans J, Philippens M, van Oorschot E (1987) Comparison of human volunteer and cadaver head-neck response in frontal flexion. Society of Automotive Engineers, paper No. 872194
62. Yoganandan N, Pintar F, Butler J et al (1989) Dynamic response of human cervical spine ligaments. Spine 14:1102–1110